Photocatalytic activity of TiO2–P25@n-TiO2@HAP composite films for air depollution

Guy Didier Fanou, Mamadou Traore, Benjamin Kouassi Yao, Andrei Kanaev, Khay Chhor

Photocatalytic activity of TiO_2-P_{25}@ n-TiO_2@HAP Composite Films for Air depollution

Guy Didier FANOU[1,2], Mamadou TRAORE[1], Benjamin Kouassi YAO[2], Andrei KANAEV[1], Khay CHHOR[1]

[1] *Laboratoire des Sciences des Procédés et des Matériaux, CNRS, Université Paris 13, Sorbonne Paris Cité, 93430 Villetaneuse, France*

[2]*Laboratoire des Procédés de Synthèse, de l'environnement et des Energies Nouvelles-LAPISEN, INPHB ; Côte d'ivoire*

Corresponding author :traore@lspm.cnrs.fr/ 0149404052 / 0149403414

Abstract

We report on an elaboration of new composite photocatalysts (TiO_2-P_{25}@ n-TiO_2@HAP) based of grafted size-selected 5nm titanium-oxo-alkoxo nanoparticles on P25-TiO_2 nanoparticles and HAP obtained by co-precipitation of salts. The 5-nm oxo-TiO_2 particles were prepared in a sol-gel reactor with rapid reagents micromixing. The photocatalytic test of ethylene degradation, in a continuous-flow fixed bed reactor, showed an increase of the photocatalytic yield for the composite photocatalysts with an addition of HAP. This result was interpreted by a synergy between adsorption and photooxidation.

Keywords: TiO_2, hydroxyapatite, composite nanoparticles, photocatalysis.

1.Introduction

The industrial, domestic and military activities are increasingly rejecting toxic materials, especially in recent decades (Jacobson 2002; Atkinson 2000; Jia 2013; Bryne et al. 1998; Guo et al. 2003). The water and air quality is decreasing which represents a serious threat for all living species. Among the possible techniques for the destruction of pollution traces are the

Advanced Oxidation Technologies (TOA), the most important of which are ozonation, the use of ultraviolet (UV), plasma degradation and photocatalysis. From 2000 to 2018, the number of publications on TOA increases by more than fourfold and reaches 7000 publications (Giwa et al, 2021). Honda and Fujishima (1972) suggested the use of TiO_2 excited by ultraviolet radiation to decompose organic pollutants.. The principle of photocatalysis involves photogeneration of electron-hole pairs. Under light excitation, the electrons (e^-) of the valence band (BV) of the TiO_2 pass to the conduction band (BC), leaving a positive charge or hole (noted h^+) in the BV. These electron-hole pairs can recombine by releasing heat, or react separately with pollutant molecules of the environment. The recombination of the photoinduced charges served to be the main shortcoming of the photocatalytic process, which can be reduced by doping of the active component and/or its integration in a composite medium. In this connection, the combination of nano-TiO_2 and HAP may be an interesting solution.

Because of a large band gap energy ~7.7 eV (λ = 160 nm), measured e.g. by Feldbach et al. (2015) and calculated by Tsukada et al. (2011), appreciable photocatalytic activity of this material cannot be expected. However, HAP was capable forming oxygen defects under UV illumination serving as active centers (Nishikawa et al. 2002) and some photocatalytic activity of HAP has been observed on the reduction of methyl mercaptan and dimethyl sulfide (Tanaka et al. 2012). The use of hydroxyapatite (HAP) as an adsorbent material is of increasing interest because of its remarkable property of ion exchange, bonding with organic molecules, low solubility in water (Iliev et al. 2007; Krestou et al. 2004; Ma et al. 1994; Qian et al 2014; Bahdod et al. 2009). Hydroxyapatite also has catalytic properties that have been studied in several fields (Monma 1982; Matsumura et al. 1984; Joris et al. 1971; Kibby et al. 1972; Bett et al., 1968; Matsumura et al. 1994; Matsumura et al. 1997; Chlala 2016): dehydrogenation, dehydration, combustion, oxidation, reforming, etc. Several studies have

51 focused on the use of the adsorption-photocatalytic coupling of the TiO_2 / HAP composite for
52 the removal of gaseous pollutants (Azouani et al. 2010a; Azouani et al. 2010b; Azouani et al.
53 2007; Benmami et al. 2006). Thus, NO adsorption was observed by Nonami et al. (2004),
54 Mitsionis et al. (2011) as well as Nasr-Esfahani et al. (2012) in photocatalytic studies.
55 However, the improvement of the gas phase photocatalytic activity due to the presence of
56 hydroxyapatite on the surface of TiO_2 is controversial; a negative or no effect can be observed
57 with regard to the process procedure and the UV wavelengths used.
58 The coupling between TiO_2 and HAP and the overall process efficiency are expected to
59 depend on the process procedure. In this work, we applied a new approach to the
60 photocatalyst synthesis by using titanium oxo-alkoxy (TOA) nanoparticles as a link between
61 TiO_2 P25 and HAP components. The photocatalytic activity of the prepared TiO_2-P_{25}@ n-
62 TiO_2@HAP materials has been evaluated.
63

64 **2. Material and Methods**
65

66 **2.1 Elaboration of TiO_2-P_{25}@ n-TiO_2**

67 The general approach to synthesize the TiO_2-P_{25}@n-TiO_2 has been proposed by Fanou et al.
68 (2016). The sol nanoparticles are prepared in the sol–gel reactor using titanium
69 tetraisopropoxide (TTIP) as a precursor. Two stock solutions: 50 cm^3 of a TTIP/propan-2-ol
70 solution and 50 cm^3 of a H_2O/propan-2-ol solution, was synchronously injected under
71 nitrogen into the turbulent mixing zone (Re = 4500) of sol–gel reactor (Azouani et al. 2010b)
72 where the oxo-TiO_2 nanoparticles were generated from hydrolysis condensation reactions.
73 The particle size can be tuned by adjusting the hydrolysis ratio $H = C_{H2O}/C_{TTIP}$, where C_{H2O}
74 and C_{TTIP} are respectively water and titanium precursor concentrations. We have prepared
75 colloids using hydrolysis ratio H = 2, which corresponds to one of stability domains of the
76 sol–gel process and enables particles size of 5.2 nm (Azouani et al. 2007). The suspended

oxoparticles solution was subsequently transferred to a glove box LABstar MBraun where they were combined slowly with TiO_2-P25 powder under stirring. The ratio 66 % of TiO_2-P25/ n-TiO_2 was the same for all prepared samples. A stable nanocoating, with a specific area of 72 m^2/g, was prepared by immobilization of nanoparticles on glass bed by dip-coating.

2.2 Elaboration of TiO_2-P_{25}@ n-TiO_2@HAP

Two types of composites were prepared by i) crystallization on the surface of the TiO_2-P25 @ n-TiO_2 of hydroxyapatite in a physiological solution SBF (CPS / HAP-SBF) ii) incorporation of hydroxyapatite in the matrix TiO_2-P25 @ n-TiO_2 (CPS / HAP).

2.2.1 Co-precipitation method

The chemicals (Sigma Aldrich) involved in this experiment are calcium nitrate $Ca(NO_3)_2,4H_2O$ (purity 99%), ammonium dihydrogen phosphate $NH_4H_2PO_4$ (purity ≥ 98%) and Ammonia (purity 99,5%). 125 ml of calcium nitrate (0.5 $mol.L^{-1}$) and 75 ml of ammonium phosphate (0.5 $mol.L^{-1}$) are mixed with vigorous stirring. Then, concentrated ammonia is added dropwise to pH≈10-10.5 to give a white precursor precipitate of HAP. After stirring for 1 hour, the suspension is filtered and stored in a hermetically sealed beaker in order to avoid carbonation due to atmospheric carbon dioxide. HAP is then mixed with the colloid suspension TiO_2-P_{25}@n-TiO_2 so as to obtain different mass percentage. The mixture of the hydroxyapatite and composite particles are immobilized by dip-coating on the 1 mm diameter glass beads for photocatalytic tests. Prepared materials are noted as CPS / HAP.

2.2.2 Simulated Body Fluid (SBF) method

This preparation method is advocated by Li et al. (1993). The chemicals were purchased from Sigma Aldrich in quantities indicated in Table 1.

In general, 250 ml of distilled water were poured into a beaker and placed in a water bath at 36.5 °C with magnetic stirring. Each reagent was then subsequently added to the reaction medium during the synthesis. The pH was adjusted to 7.25 using 1N HCl. At the end, the volume of the solution was completed to 500 mL with distilled water and stored in a refrigerator at 5-10 °C. The crystallization of hydroxyapatite on TiO_2-P25 @ n-TiO_2 composite was carried out by placing the composite samples and the SBF solution in contact under slight agitation. The crystallization time varies from 30 min to 5h. Longer calcination times were also used in the preparation and specified if applicable. Prepared materials are noted as CPS / HAP-SBF.

2.3. Photocatalyst Characterization

The prepared samples were structurally characterised by X-ray diffraction XRD (INEL XRG 3000) using CuKα radiation with Nickel filter. The surface morphology of photocatalyst was examined by SEM JEOL JSM 64400F with acceleration voltage of 10 kV. Raman spectra were measured at 516 nm using micro-Raman high-resolution HR800 installation (HORIBA JobinYvon) with the spectral and spatial resolution respectively 0.25 cm^{-1} and 5 μm. The scattered light is collected by Peltier cooled CCD camera in a backscattering configuration. The photocatalytic activity of the prepared samples was tested in a continuous-flow fixed-bed reactor on ethylene decomposition. A gas flow of pollutant (120 ppm) mixture with dry air and flow rate of 7.5 mL/min passes through a reactor tube of 6-mm diameter and 35 cm length made of glass transparent in the UV-A spectral range (Benmami et al. 2005; Tieng et al. 2011). The glass beads coated photocatalyst samples were filled the reactor tube of 15 cm length around the middle. Inside the tube, just after the glass bead, a chromel / alumel thermocouple monitors the temperature. The tube is surrounded at a radial distance of 3 cm by six 8-W lamps of 29 cm length emitting at 362 nm ($\Delta\lambda_{hwfm}$ = 22 nm). During the experiments,

the reactor is cooled by compressed air stream. Ethylene concentrations before (C_{in}) and after (C_{out}) the photocatalytic reactor were monitored by online gas chromatography (Varian 191 CP 3800) equipped with a capillary column (HP-PLOT/Q) and a flame ionization detector FID. Before turn on the UV lamps, one hour period is applied for the stabilization of Ethylene concentrations and the gas inlet stream temperature at 25 °C. Two injection loops of 250 µL and heated at 80 °C allow measurements of pollutant concentration in continuous mode. The reactor yield (or ethylene conversion) is calculated according to the formula: $\eta(\%) = (C_{in}-C_{out})/C_{in}\times 100$. The column temperature and flow rate of the carrier gas (N_2) were respectively 50 °C and 5 mL/min.

3. Characterization

3-1. X-ray diffraction

The X-ray plots of pure hydroxyapatite (figure 1) show well-defined peaks indicating that the solids are well crystallized.

In the range of 2θ between 25 and 35 °, they reveal clear diffractions of the (002) planes at 25.7 ° and those of the (211), (300), and (202) planes at 31.6, 32, 7 ° and 33.9 ° respectively. All these planes can be indexed in the hexagonal space group system P63 / m (Nathanael et al. 2010). The average size of the crystallites was estimated using the Sherrer formula (Smith 1989) and the Bragg reflection of the (002) planes. These parallel planes with the $\vec{c}$ axis represent the preferential direction of growth of the hydroxyapatite.

$$d = \frac{k\lambda}{b(2\theta)\cos\theta}$$

d is the diameter of the crystallites (Å), k is a constant (0.9), λ is the incident wavelength (Å), θ is the Bragg angle (degree) and b is the half width. recorded peak height expressed in radians.

The calculated value of d is close to 21 nm for the sample treated at 100 ° C. and 22.5 nm for that calcined at 450 ° C.

The X-ray diffraction patterns of the samples of the TiO_2-P25 @ n-TiO_2 composite containing a dispersion of HAPs are shown in Figure 2.

The spectra show a presence of crystallized HAP in the material. The intensity of the most intense HAP peaks around 31.5 ° increases with the increase in its mass content in the material. They appear clearly in the sample diagram with 30% PAH.

3-2. Raman spectroscopy

The vibrational study by Raman scattering was recorded on the powders of the following samples:

i) Pure hydroxyapatite treated at 450 ° C.

ii) TiO_2-P25 @ n-TiO_2 / PAH noted CPS / HA with a mass content equal to 3 and 5% of incorporated PAH.

The spectrum of hydroxyapatite is shown in Figure 3.

The frequency range between 400 and 1200 cm^{-1} characterizes the diffusion bands of the $(PO_4)^{3-}$ group. The peaks observed around 430 and 449 cm^{-1} can be attributed to the deformation vibration $\upsilon 2$. The Raman bands at 580, 592 and 610 cm^{-1} correspond to the triple degenerate vibrational mode $\upsilon 4$. The symmetrical elongation vibration mode υ_1 of the $(PO_4)^{3-}$ group appears as a very intense peak located at 962 cm^{-1}. This diffusion band is characteristic of the structure of hydroxyapatite (Smeulders, 2001). The antisymmetric vibration υ_3 can be associated with the diffusion bands observed at 1032, 1048 and 1079 cm^{-1}. Figure 4 shows the

175 Raman spectra of the TiO2-P25 @ n-TiO2 / HAP (CPS / HAP) composite with a mass
176 content of 3 and 5% PAH.
177
178 The spectra obtained clearly show three Raman bands at 399, 516 and 642 cm^{-1} of the anatase
179 of the composite. As for the hydroxyapatite, because of its low concentration in the matrix (3
180 and 5%) the intensity of the diffusion bands is very weak making the observation difficult.
181 The only detectable peak is 962 cm^{-1} attributed to the vibrational mode υ_1 of the $(PO_4)^{3-}$
182 group.
183
184 **4. Photocatalytic activity**
185
186 **4-1. Co-precipitation method**
187 The photocatalytic tests were measured on the samples of 0.5% and 1% by weight of
188 hydroxyapatite with the references CPS / HAP-0.5 and CPS / HAP-1 respectively. Figure 5
189 shows the evolution of photocatalytic activity of ethylene degradation.
190
191 The conversion of ethylene to CPS / HAP-0.5, CPS / HAP-1 shows a rapid increase for 20
192 min under UV radiation. As Tieng et al have already observed (2011), the warm up time of
193 UV lamps was too short (Figure 6a) to account for this behavior. The temperature increases
194 from 25 °C to 46 ± 2 °C in about 3 min. Moreover no photolysis of ethylene is observed
195 (Figure 6b). The delay in the achievement of the asymptotic ethylene conversion has been
196 previously explained by the formation of non-volatile intermediate reaction products, assigned to the
197 oxidized polymeric hydrocarbons: furan and furfural oligomers Ol_N with N=6÷8 (Tieng et al. 2019).
198 After this step, the photocatalytic yield reaches a stable steady state corresponding to a
199 conversion value η greater than that of the reference composite: 12% for CPS / HAP-1 and

200 6% for CPS / HAP-0.5. The first order rates of the pollutant decomposition in Figure 7, which
201 reflects the intrinsic photocatalyst activity (Fanou et al. 2016), showed a linear proportionality
202 to the HAP content. It begins however from a non-zero value, characteristic of the pure titania
203 activity, increasing by ~50% at 1wt% of HAP.
204
205 This enhancement might be associated with: i) strong adsorption capacity of hydroxyapatite
206 with respect to the pollutant and the secondary reaction products likely to form during the
207 photocatalytic reactions (Hauchecorne et al. 2011), ii) better availability of active sites
208 because of elimination of poisons by adsorbance on the composite surface , and iii) charge
209 separation efficiency enhancement in the composite. Mitsionis et al. (2011) have reported that
210 the formation of OH^{o} radicals is greater onto HAP / TiO_2 composite than TiO_2 alone. In the
211 same time, the band gap energy of HAP/TiO_2 composite E_g=3.08 eV (Kamat 2002) has been
212 reported to be insignificantly lower compared with pure titania (3.12 eV), whereas that of
213 HAP reported by Feldbach et al. (2015) and Lopez et al. (2013) was significantly larger: 7.7
214 eV and >6 eV respectively. Accordingly, synergistic effect between adsorbing and active sites
215 could be responsible for the enhanced activity of the composite. The following scenario
216 highlighting the synergistic action of these two components, composite and adsorbent, can be
217 described as follows: the molecules of the pollutant are additionally adsorbed by HAP and
218 then migrate along the composite surface to the active nanoparticles where they react. The
219 secondary products, if formed, can be advantageously captured by HAP discharging active
220 sites to be decomposed on a later stage.
221
222 **4-2. SBF method**
223 Figure 8 shows the results of the photocatalytic activity of the films prepared with a
224 crystallization time of 30 min.

225 The obtained results indicate that the ethylene conversion η increases rapidly for about 20
226 minutes of irradiation to reach a maximum of 3% to 5% higher than that of the reference
227 (TiO_2-P25 @ n-TiO_2). We also explained this behavior by the thermal activation of the
228 material following the rise of temperature. It then shows a slow decrease to a lower value than
229 that of the untreated sample after about 40 minutes. This behavior is fairly reproducible for
230 the three samples. Different reasons can explained this behavior : (i) scattering of the incident
231 light by the surface particles (ii) e^-/h^+ charge transfer blocking at the composite-
232 hydroxyapatite interface of the composite to the adsorbed ethylene (Feldbach et al. 2015;
233 Tsukada et al. 2011), iii) poisoning of sites material assets by the presence of products from
234 the elaboration stage.

235 In order to confirm these hypotheses, we studied the influence of the crystallization
236 time on the photocatalytic activity shown in Figure 9. The results show the similar behavior
237 observed on Figure 8 and the maximum ethylene conversion is also obtained at the same time
238 (30-40 min).

239

240 We observe that the prolonged crystallization time decreases the photocatalytic
241 activity of the composite material. This reduction in photocatalytic performance is important
242 and varies from 5% (30 min) to 75% for a crystallization time of 5 h. These results support the
243 explanations we have advanced above: hydroxyapatite on the surface, increase the scattering
244 of the incident light and reduce the charges transfer at the interface and the crystallization
245 products can poison the photocatalyst.

246 The different performances of the two prepared TiO_2-P_{25}@ n-TiO_2@HAP materials
247 (Figures 5 and 8) can be explained by their probable structure. Hydroxyapatite crystals
248 deposited on the surface of TiO_2-P_{25}@ n-TiO_2 is obtained by the SBF method. In this case, an
249 increase of crystallization time causes a decrease of the photocatalytic activity. Whereas,

when hydroxyapatite crystals are incorporated in the TiO_2-P_{25}@ n-TiO_2 matrix, it is dispersed in the composite and can create a synergistic effect of hydroxyapatite on the photooxidation properties of the photocatalyst.

4. Conclusion

Two families of new composite photocatalysts were prepared by crystallization on the surface of the TiO_2-P25 @ n-TiO_2 of the hydroxyapatite in a physiological solution SBF and by incorporation of hydroxyapatite in TiO_2-P25 @ n-TiO_2 matrix. Both HAP and TiO_2 conserve own crystallinity in the material. The photocatalytic yield (gas phase conversion of ethylene) of the material obtained by co-precipitation was increased with an increase of the HAP content, indicating the synergy between two components. On the other hand, the prolonged crystallization time of the composite in SBF has a negative effect on the photocatalytic yield.

Declarations

Ethics approval and consent to participate :

Not applicable

Consent for publication :

Not applicable

Availability of data and materials :

The datasets used and/or analysed during the current study are available from the corresponding author on reasonable request.

Competing interests :

The authors declare that they have no competing interests

Funding :

Not applicable

Authors' contributions :

All authors (Guy Didier FANOU, Mamadou TRAORE, Benjamin Kouassi YAO, Andrei KANAEV and Khay CHHOR) contributed to the study conception and design. Material preparation, data collection and analysis were performed by Guy Didier FANOU. The first draft of the manuscript was written by Mamadou TRAORE and other authors (Guy Didier FANOU, Benjamin Kouassi YAO, Andrei KANAEV and Khay CHHOR) commented on previous versions of the manuscript. All authors (Guy Didier FANOU, Mamadou TRAORE, Benjamin Kouassi YAO, Andrei KANAEV and Khay CHHOR) read and approved the final manuscript.

Acknowledgements :

Not applicable

298 **References**

299 -Atkinson R. (2000), Atmospheric chemistry of VOCs and NO_x, Atmos. Environ. 34 : 2063–
300 2101.

301 -Azouani R., Michau A., Hassouni K., Chhor K., Bocquet J.-F., Vignes J.-L., Kanaev A.
302 (2010), Elaboration of pure and doped TiO_2 nanoparticles in sol–gel reactor with turbulent
303 micromixing: Application to nanocoatings and photocatalysis, Chem. Eng. Res. Des. 88 :
304 1123–1130.

305 -Azouani R., Soloviev A., Benmami M., Chhor K., Bocquet J.-F., Kanaev A. (2007), Stability
306 and growth of titanium-oxo-alkoxy $Ti_xO_y(OiPr)_z$ clusters, J. Phys. Chem. C. 111 : 16243–
307 16248.

308 -Azouani R., Tieng S., Chhor K., Bocquet J.-F., Eloy P., Gaigneaux E. M., Klementiev K.,
309 Kanaev A. (2010), TiO_2 doping by hydroxyurea at the nucleation stage: towards a new
310 photocatalyst in the visible spectral range, Phys. Chem. Chem. Phys. 12 : 11325–11334.

311 -Bahdod A., El Asri S., Saoiabi A., Coradin T., Laghzizil A. (2009), Adsorption of phenol
312 from an aqueous solution by selected apatite adsorbents: Kinetic process and impact of the
313 surface properties, Water Res. 43 : 313–318.

314 -Benmami M., Chhor K. and Kanaev A. (2005) Supported nanometric titanium oxide sols as a
315 new efficient photocatalyst, J Phys Chem B, 109: 19766- 19771.

316 -Benmami M., Chhor K. and Kanaev A. (2006), High photocatalytic activity of monolayer
317 nanocoatings prepared from non-crystalline titanium oxide sol nanoparticles, Chem. Phys.
318 442 : 552–557.

319 -Bett J.A., Hall W.K. (1968), The microcatalytic technique applied to a zero order reaction:
320 The dehydration of 2-butanol over hydroxyapatite catalysts, J. Catal. 10 : 105–113.

-Byrne J.A., Eggins B. R., Brown N.M.D., McKinney B., Rouse M. (1998), Immobilisation of TiO_2 powder for the treatment of polluted water, Appl. Catal. B Environ. 17 : 25–36.

-Chlala D., Labaki M., Giraudon J., Lamonier J. (2016), Toluene total oxidation over Pd and Au nanoparticles supoorted on hydroxyapatite, Comptes Rendus Chimie, 19 : 525-537.

-Fanou G.D., Yao B., Cheng K., Brinza O., Traore M., Kanaev A., Chhor K. (2016), "Elaboration of novel nanoparticulate TiO_2-P25@nTiO_2 composite for Catalysis", International Journal of Advanced Applied Physics Research 3 : 19-25.

-Feldbach E., Kirm M., Kotlov A., Mägi H. (2015), Luminescence Spectroscopy of Ca-apatites under VUV Excitation, User Rep. Mater. Sci. Httpphoton-Sci. Desy . 17 : 122–123.

-Fujishima A., Honda K. (1972), TiO_2 photoelectrochemistry and photocatalysis, Nature. 238 : 37–38.

-Giwa A., Yusuf A., Balogun H. A, Sambudi N. S., Bilad M. R., Adeyemi I., Chakraborty S. Curcio S. (2021), Recent advances in advanced oxidation processes for removal of contaminants from water: A comprehensive review, Process Safety and Environmental Protection, 146 : 220-256

-Guo F.Q., Okamoto M., Crawford N. M. (2003), Identification of a plant nitric oxide synthase gene involved in hormonal signaling, Science. 302 : 100–103.

-Hauchecorne B., Tytgat T., Verbruggen S.W., Hauchecorne D., Terrens D., Smits M., Vinken K., Lenaerts S. (2011), Photocatalytic degradation of ethylene: An FTIR in situ study under atmospheric conditions, Appl. Catal. B Environ. 105 : 111–116.

-Iliev V., Tomova D., Bilyarska L., Tyuliev G. (2007), Influence of the size of gold nanoparticles deposited on TiO_2 upon the photocatalytic destruction of oxalic acid, J. Mol. Catal. Chem. 263 : 32–38.

-Jacobson M.Z. (2002), Atmospheric pollution: history, science, and regulation, Cambridge University Press.

-Jia Z. (2013), Elaboration des matériaux composites nanostructurés Ag, Au/TiO_2 pour la dépollution des effluents gazeux avec une activation par plasma, Université Paris 13.

-Joris S. J., Amberg C. H. (1971), J. Phys. Chem. , 75 : 316

-Kamat P.V. (2002), Photophysical, photochemical and photocatalytic aspects of metal nanoparticles, J. Phys. Chem. B. 106 : 7729–7744.

-Kibby C.L., Lande S.S., Hall W.K. (1972), Tracer studies of acid-catalyzed reactions. XI. Stereoselectivity in alcohol dehydration over hydroxyapatite and alumina catalysts, J. Am. Chem. Soc. 94 : 214–220.

-Krestou A., Xenidis A., Panias D. (2004), Mechanism of aqueous uranium (VI) uptake by hydroxyapatite, Miner. Eng. 17 : 373–381.

-Li P., Nakanishi K., Kokubo T., de Groot K. (1993), Induction and morphology of hydroxyapatite, precipitated from metastable simulated body fluids on sol-gel prepared silica, Biomaterials. 14 : 963–968.

-Lopez L., Daoud W.A., Dutta D., Panther B.C., Turney T.W. (2013), Effect of substrate on surface morphology and photocatalysis of large-scale TiO 2 films, Appl. Surf. Sci. 265 : 162–168.

-Ma Q.Y., Traina S.J., Logan T.J., Ryan J.A. (1994), Effects of aqueous Al, Cd, Cu, Fe (II), Ni, and Zn on Pb immobilization by hydroxyapatite, Environ. Sci. Technol. 28 : 1219–1228.

-Matsumura Y., Kanai H., Moffat J.B (1997), Catalytic oxidation of carbon monoxide over stoichiometric and non-stoichiometric hydroxyapatites, J. Chem. Soc. Faraday Trans. 93 : 4383–4387.

-Matsumura Y., Moffat J.B. (1994), Partial Oxidation of Methane to Carbon-Monoxide and Hydrogen with Molecular-Oxygen and Nitrous-Oxide over Hydroxyapatite Catalysts, J. Catal. 148 : 323–333.

-Matsumura Y., Moffat J.B. (1996), Methanol adsorption and dehydrogenation over stoichiometric and non-stoichiometric hydroxyapatite catalysts, J Chem Soc Faraday Trans. 92 : 1981–1984.

-Mitsionis A., Vaimakis T., Trapalis C., Todorova N., Bahnemann D., Dillert R. (2011), Hydroxyapatite/titanium dioxide nanocomposites for controlled photocatalytic NO oxidation, Appl. Catal. B Environ. 106 : 398–404.

-Monma H. (1982), Catalytic behavior of calcium phosphates for decompositions of 2-propanol and ethanol, J. Catal. 75 : 200–203.

-Nasr-Esfahani M., Fekri S. (2012), Alumina/TiO2/hydroxyapatite interface nanostructure composite filters as efficient photocatalysts for the purification of air, React. Kinet. Mech. Catal. 107 : 89–103.

-Nathanael A. J., Mangalaraj D., Chen P.C., Ponpandian N. (2010), Mechanical and photocatalytic properties of hydroxyapatite/titania nanocomposites prepared by combined high gravity and hydrothermal process, Compos. Sci. Technol. 70 : 419–426.

-Nishikawa H., Omamiuda K. (2002), Photocatalytic activity of hydroxyapatite for methyl mercaptane, J. Mol. Catal. Chem. 179 : 193–200.

-Nonami T. (2004), Apatite-Coated Titanium Dioxide Photocatalyst for Air Purification, Catal. Today. 96 : 113–118.

-Qian G., Li M., Wang F., Liu X. (2014), Removal of Fe3+ from Aqueous Solution by Natural Apatite, J. Surf. Eng. Mater. Adv. Technol.

-Smeulders D. E., Wilson M.A., Armstrong L. (2001), Insoluble organic compounds in the Bayer process, Ind. Eng. Chem. Res. 40 : 2243–2251

-Smith K. (1989), Modern Powder Diffraction"; in Review in Mineralogy, Edited by D. L. Bish and J. E. Post. Mineralogical Society of America,Washington, DC, 20 : 183.

-Tanaka H., Tsuda E., Nishikawa H., Fuji M. (2012), FTIR studies of adsorption and photocatalytic decomposition under UV irradiation of dimethyl sulfide on calcium hydroxyapatite, Adv. Powder Technol. 23 : 115–119.

-Tieng S, Kanaev A and Chhor K. (2011) New homogeneously doped Fe(III)-TiO_2 photocatalyst for gaseous pollutant degradation, J Appl Catal A 399: 191-197.

-Tieng S, Jia Z., Diaz-Gomez Trevino A. P., Eloy P., Giagneaux E. M., Chhor K., Kanaev A. (2019) Major non-volatile intermediate products of photo-catalytic decomposition of ethylene, Journal of Catalysis 374: 328-334.

-Tsukada M., Wakamura M., Yoshida N., Watanabe T. (2011), Band gap and photocatalytic properties of Ti-substituted hydroxyapatite: comparison with anatase-TiO 2, J. Mol. Catal. Chem. 338 : 18–23.

406 **FIGURES**

407

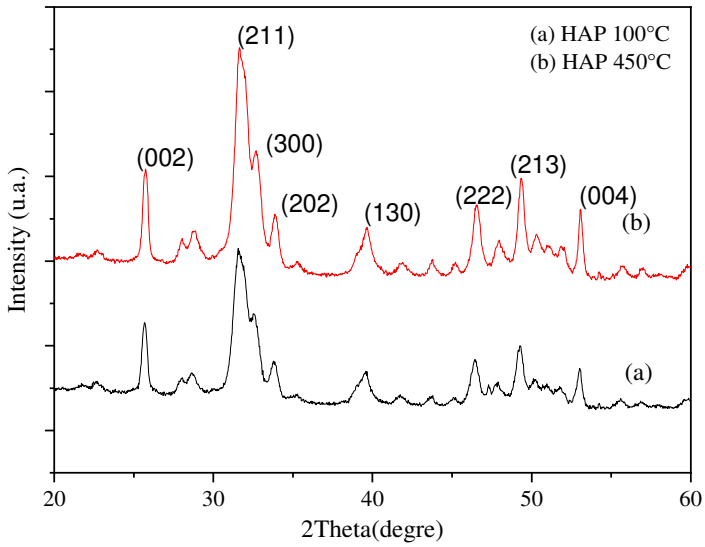

408

409 *Fig. 1: Heat-treated hydroxyapatite diffraction patterns at 100°C (a) and 450°C (b).*

410

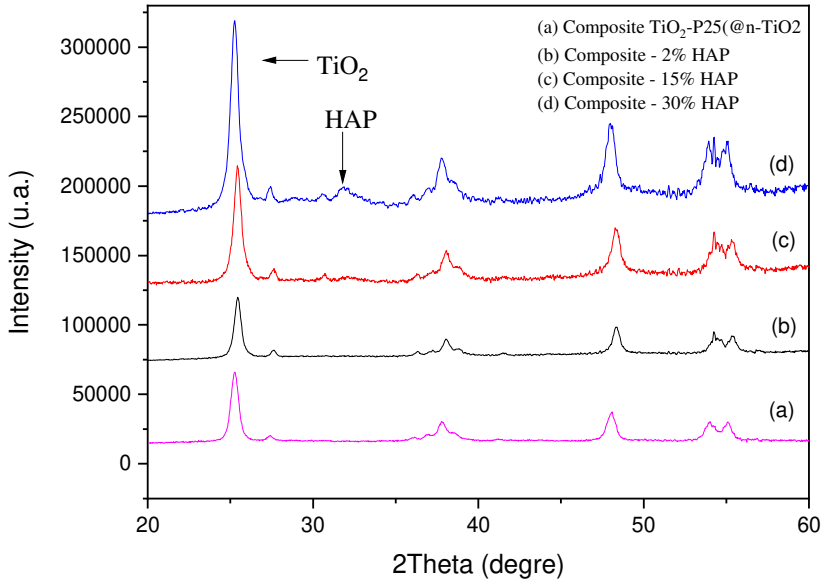

411

412 *Fig. 2: X-ray diffractograms of samples of TiO2-P25 @ n-TiO2 / HAP composite treated with*
413 *different mass compositions of hydroxyapatite (a) 0%, (b) 2% (c) 15% and (d) 30%.*

414

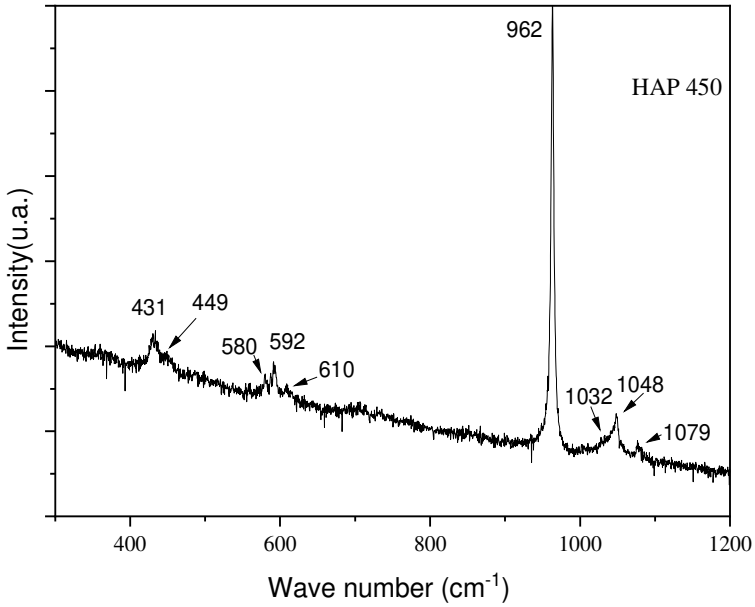

415

416 *Fig. 3: Raman spectrum of hydroxyapatite treated at 450 ° C recorded with excitatory*

417

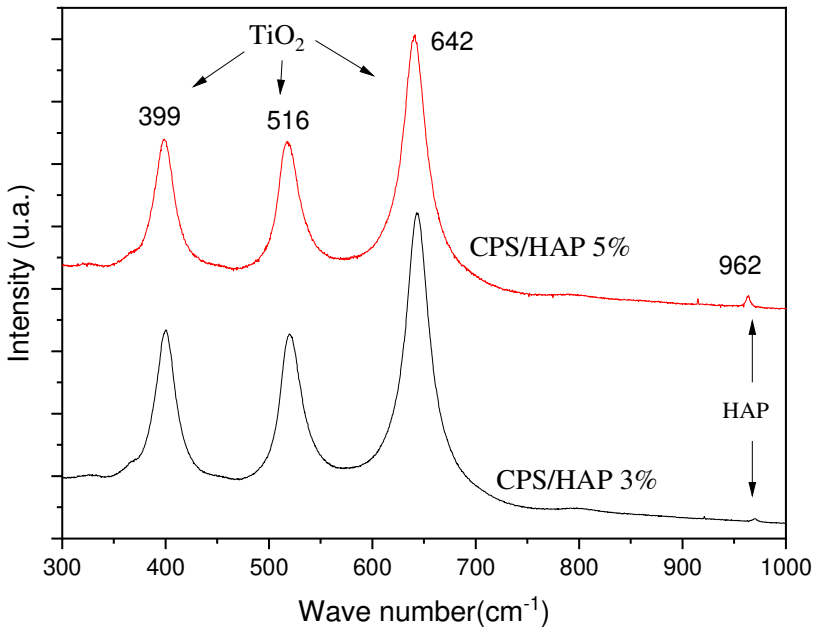

418

419 *Fig. 4: Raman spectra of two CPS / PAH samples loaded with 3 and 5% PAH and treated at*

420 *450 ° C for 4 h.*

421

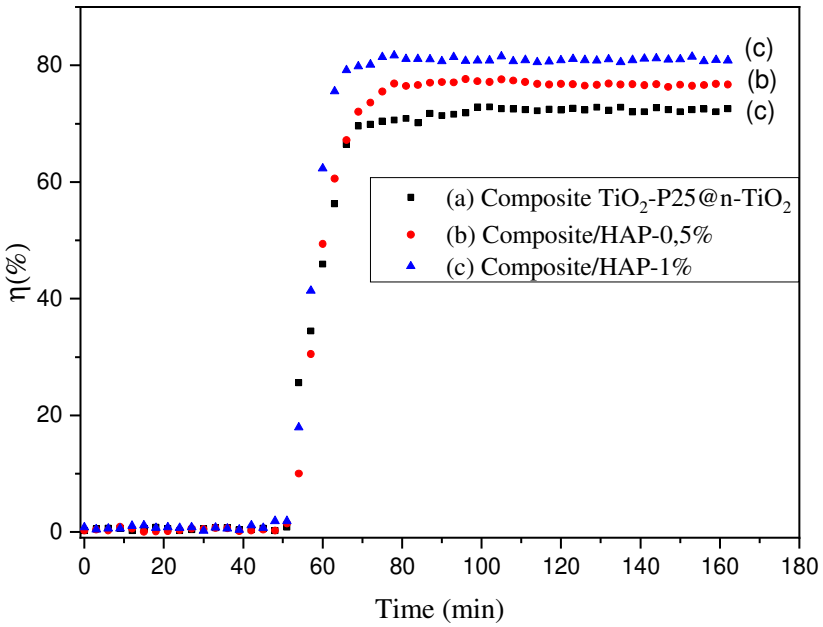

422

423 *Fig. 5: Evolution of the photodegradation of ethylene by CPS / HAP-0.5 and CPS / HAP-1 as*
424 *a function of the irradiation time. The conversion rate of ethylene by the untreated composite*
425 *is given for comparison. (λ = 360 nm, ethylene 150 ppm, flow rate 10 mL.min^{-1}).*

426

427

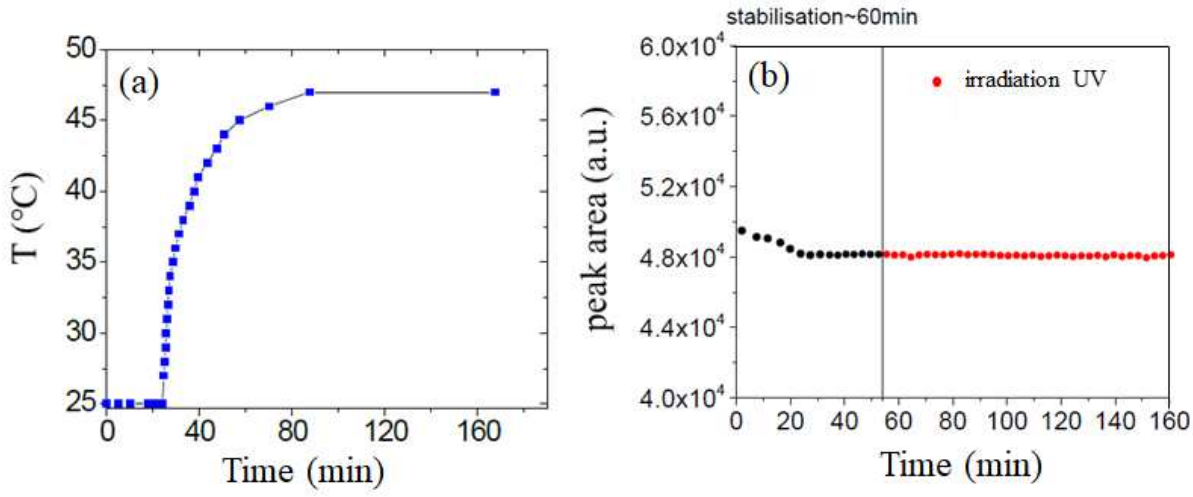

428

429 *Fig. 6: Temperature evolution during photocatalytic tests (a) and Ethylene concentration*
430 *evolution under UV irradiation without photocatalysts (b).*

431

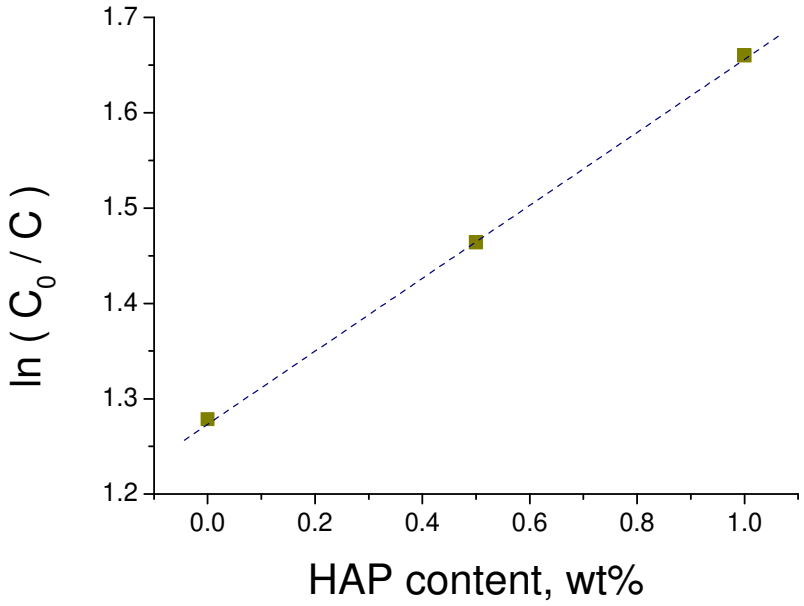

Fig. 7: Photocatalytic activity as a function of HAP doping.

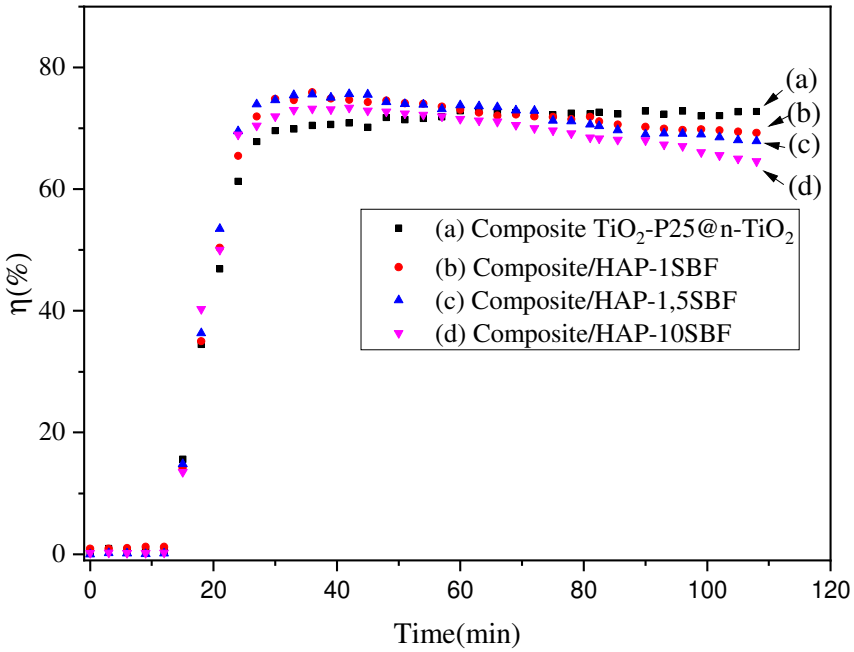

Fig. 8: Evolution of the photodegradation of ethylene by different CPS / HAP-SBF as a function of the irradiation time. The conversion rate of ethylene by the untreated composite is given for comparison. (λ = 360 nm, ethylene 150 ppm, flow rate 10 mL.min^{-1}).

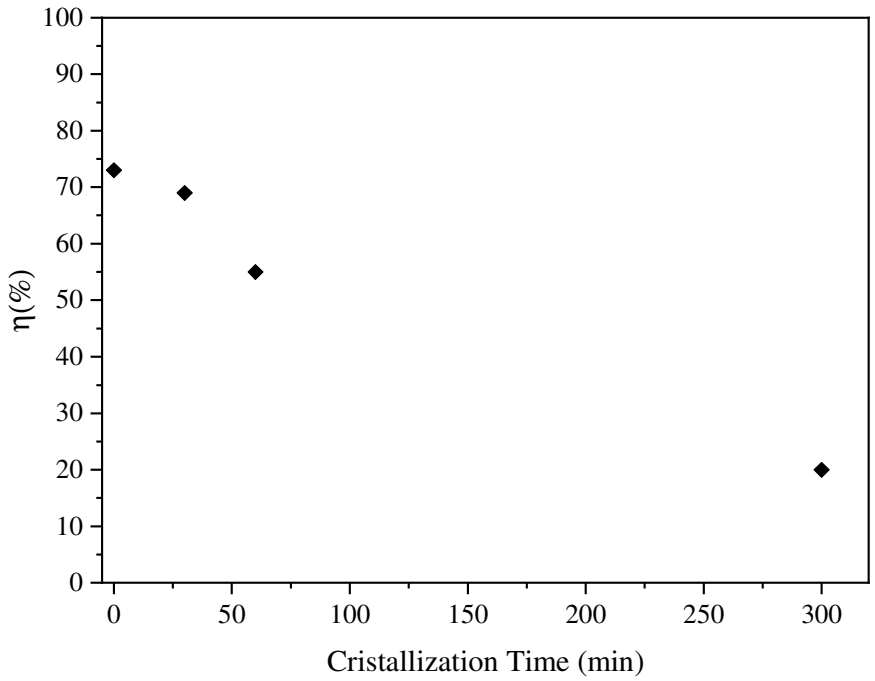

Fig. 9: Photodegradation of ethylene by CPS / HAP-1SBF as a function of the crystallization time. (λ = 360 nm, ethylene 150 ppm, flow rate 10 mL.min^{-1}).